Posture and Body Movement Effects on Behavioral Biometrics for Continuous Smartphone Authentication

Nicholas Cariello, Robert Eslinger, Rosemary Gallagher, Isaac Kurtzer, Paolo Gasti, Kiran S. Balagani

***Abstract*—Continuous authentication aims to authenticate users at regular intervals post-login, typically using biometric features that capture the user's behavior. One of the drawbacks of continuous authentication is that it usually introduces a high authentication latency, i.e., behavioral features need to be captured for 45–120 seconds in order to achieve acceptable authentication error rates. In this paper, we take a step towards addressing this problem by harnessing 3D motion capture data and creating an extensive set of body motion and posture features with the goal of achieving low authentication error rates with short (1–5 second) authentication latencies. To evaluate our features, we collected a dataset from 39 users engaged in a set of smartphone tasks performed in a 3D motion capture studio. To collect our data, we placed 41 IR-reflective markers on the subjects' body and 3 on the smartphone. The markers were tracked by 3D motion capture cameras. During data collection, subjects were either walking along a pre-determined path or sitting. We show that our features can lead to a low equal error rate (EER) of 6.4% with 1-second latency, and 5.4% with 5-second latency. In contrast, under the same experimental settings, swipe and phone-movement features alone led to an EER of 15.7% for a 60-second authentication latency. While our features demonstrate the potential to achieve low authentication error with very low authentication latencies, we envision that in practice these features will be collected using standard smartphone sensors and consumer-grade wearable devices. We believe that our results hold transformative potential, because they shift continuous authentication from a reactive (i.e., detection is successfully performed well into the attack) to a proactive security measure (i.e., detection happens as the attack starts). As part of our contributions, we have made the dataset used in this paper publicly available.**

***Index Terms*—Behavioral Biometrics, Smartphone Authentication, Continuous Authentication, 3D Motion Capture**

I. Introduction

THE goal of continuous smartphone user authentication is to determine whether the genuine user is operating a device post-unlock. Biometric modalities suitable for continuous authentication must be collectable without disrupting the user's workflow [1]. Prior work has demonstrated that several naturally-occurring smartphone user behaviors can be reliably used for continuous authentication. These include touchscreen gestures (swipes and taps) [2], [3], [4], [5], [6], [7], keystroke dynamics [8], [9], [10], [11], phone-movement [12], [13], [14], [15], gait [8], [16], [17], [18], [19], face recognition [20], and more recently, acoustic reflections [21].

With all smartphone behavioral modalities there is a trade-off between *authentication latency*, defined as the time needed to collect enough behavioral data to trigger the next authentication event, and the resulting *authentication error rate*, defined as the percentage of errors (false positives and false negatives) made by the authentication system.

Longer authentication latencies increase the time between a successful impersonation attack and its detection. As a result, shorter authentication latencies are preferred. However, because of the inherent noise in smartphone behavioral features, longer authentication latencies tend to result in lower error rates. Therefore, continuous authentication systems based on smartphone behavioral features often struggle to strike the right balance between authentication the latency and the authentication error rate.

To achieve acceptable authentication error rates, most modalities tend to have authentication windows in the order of 45–120 seconds [21], [22], [23]. This is far from ideal, because it means that the authentication system will typically allow the adversary to operate the smartphone for an amount of time that could be sufficient to cause significant damage.

With this work, we identify a catalog of features that can be used to reduce authentication latency to 1–5 seconds while maintaining error rates in line with the current state of the art [3]. We argue that a system that is able to cut authentication latency from 45 to 5 seconds is a game-changer in terms of security, because it can effectively *prevent* the attack, rather than merely *identifying* it once the damage has been done.

To achieve this goal, we focus on user posture and body movement during swipe. To capture this information, we use a 3D motion capture system that provides a fine-grained representation of the user's body in space. We then combine features extracted from motion capture data with smartphone touchscreen swipe and phone-movement features. Our results show that posture and body movement features lead to a substantial reduction in authentication latency without sacrificing on error rates. For instance, in the sitting posture, we were able to achieve an equal error rate (EER) of 5.4% for a 5-second authentication window using our features with a Random Forest verifier. In the same setting, swipe and hand phone-movement features alone led to an EER of 14.6% for a 60 second window. Similarly, for walking posture we achieve 6.9% EER using our features, compared to 15.7% EER when using only swipe and phone-movement features. To our knowledge, this is the first work that demonstrates that: (1) posture and body movement behavioral features can be harnessed to reliably authenticate users, and (2) when using appropriate combinations of features, smartphone behavioral authentication can achieve low error rates with authentication latencies as low as 1–5 seconds.

This work focuses on the foundational aspects of posture and body movement based behavioral authentication. We do not expect that, in real-world settings, body posture/movement

All authors are with New York Institute of Technology (NYIT).

This work was supported by the National Science Foundation under award CNS 1814846.

features will be extracted for the purpose of continuous authentication using 3D motion capture equipment. Our goal in using this equipment is to determine *which features*, when accurately collected, result in low authentication latency *and* low error rates. In practice, we envision that these features will be collected using standard smartphone sensors and other wearable devices (see Section V for examples and discussion of how these features can be estimated in the real-world).

A. Summary of Contributions

The main contributions of this work are summarized next:

- We demonstrate that posture and body movement can be reliably used to continuously authenticate smartphone users.
- By augmenting traditional swipe and phone-movement features on smartphones with body posture and movement features, we are able to reduce authentication latency to 3–5 seconds while maintaining error rates in line with the current state of the art. This is a significant improvement over the 45–120 second authentication latencies common in prior behavioral authentication work, to the point that it transforms continuous authentication from a reactive to a proactive security measure.
- To evaluate our features, we collected a unique dataset from 39 users while they were performing smartphone tasks. The dataset includes a total of 29,827 swipes, as well as keystroke data, and has been made publicly available by the authors (see https://www.nyit-lamp.com/dataset/dataset4/).
- We perform an extensive analysis of the features we use, including ranking based on mutual information and the relationship between anthropometric characteristics, i.e., physiological measurements and proportions of the human body, and the performance of the features that capture them.
- We identify the body region combination that provides the most valuable information for body posture- and movement-based smartphone user authentication.

B. Organization

The rest of this paper is organized as follows. We review related work in Section II. In Section III, we present our experimental setup and the dataset we collected. In Section IV, we report our results. In Section V, we present existing studies that demonstrate body posture and movement captured using smartphones and wearable devices. We conclude in Section VI.

II. Related Work

There is a substantial body of work on continuous authentication. In this section, we focus on the most relevant work in smartphone behavioral biometrics, human activity recognition related to security applications, and motion capture biometrics. In Table I, we summarize relevant related work, and the corresponding datasets used in each study.

Smartphone Behavioral Biometrics. Behavioral biometrics can be used to continuously authenticate a user on their mobile device based on their behavior [24], [25]. Behavioral signals, such as keystroke dynamics, gait, and swipes, can be derived from sensors on smartphones capable of accurately measuring touch interactions, the acceleration and rotation of the device.

Chao et al. [3] explored the use of swipes using multiple fingers and varying swipe lengths. Their work shows that swipes can be used to identify users, with the best performing swipe being with the right thumb with an EER of 13.5%. They also demonstrated that a fusion of swipes, specifically a leftward swipe with the right thumb and a leftward swipe with the left thumb, yield an improved EER of 8.1%. Shen et al. [5] explore swipe-based authentication using a dataset of 71 users using a feature set of long touches on smartphones, and report an EER of 8.87% at 6.11 seconds or 5 swipes.

Sitová et al. [22] utilized smartphone accelerometer and gyroscopic sensors to extract Hand, Movement, Orientation and Grasp (HMOG) features. Their results showed HMOG features performed better during walking rather than sitting, and that phone-movement features perform better during touchscreen interaction. Shen et al. [26] perform multi-modal behavioral authentication using phone-movement data collected during swipe actions, expanding on their original feature set by including smartphone movement with gyroscope and accelerometer data. In their experiments over a dataset of 102 subjects, they achieve EERs between 4.93% and 26.74% depending on the authentication window size, which was between 0.73 and 16.32 seconds.

Li et al. [27] demonstrated that data augmentation can be used to achieve a behavioral authentication EER of 8.33% across a 5-second window using multiple smartphone interaction behaviors extracted from the HMOG dataset [22]. However, it is unclear what the EERs were for each individual behavior, such as swiping, typing, and other smartphone activities. Ray-Dowling et al. [28] evaluate a set of swipe and phone-movement features on two public smartphone datasets: BB-MAS [29], and HMOG [22]. They were able to achieve low equal error rates of 0.2% and 1.5% respectively, using 25 seconds of motion data and about 2.5–8 minutes of swipe data. Garbuz et al. [2] demonstrated that vertical swipes can be used as a behavioral biometric in conjunction with phone-movements, successfully identifying impostors after 2–3 gestures and accidentally blocking the legitimate user after 115–116 gestures. Kumar et al. [12] explored fused biometrics, and demonstrated that phone-movement in conjunction with swiping and typing can be used to authenticate users. They achieved a best accuracy of 93.33%.

Human Activity Recognition. Human activity recognition (HAR) has been used in a variety of applications, including healthcare [30], sports [31], and security [32], [33], [17], [34], [35], [36], [37]. In the latter scenario, HAR has been used to detect and prevent unauthorized access to computers. Chatterjee et al. [37] demonstrated that it is possible to use posture as a biometric by capturing temporal postural signals and applying S-transforms to determine characteristic features. Their work shows that they were able to successfully identify users with an authentication accuracy of 94–95%.

Motion Capture Biometrics. Motion capture is the process of recording the motion of objects and people in space. Motion capture is used in a variety of scenarios, including entertainment, sports, and security. In the context of user authentication and identification, examples include [38], [39], [40], [41], [42], [43]. In particular, Munsell et al. [41] captured motion data using a Kinect RGBD sensor, showing the effectivess of anthropometric features for low-cost user identification. They report an average EER of 13%. Similarly, Derlatka et al. [43] demonstrated the use of motion capture for continuous authentication, achieving a similar EER of 13% also using Kinect sensors with accelerometers. Muhammad et al. [42] demonstrated the feasibility of identifying users based on gait with data captured from a smartphone. They achieved an EER of 13%, which aligns with the state of the art for video motion capture. This demonstrates the viability of motion capture not only in identifying users but also as a meaningful biometric.

To our knowledge, this paper is the first to explore the use of posture and body movement features combined with swipe signals for the purpose of continuous behavioral authentication of smartphone users.

III. Experiment Setup

To evaluate the features presented in this paper, we collected data from 39 subjects between the ages of 18 and 35.[1] The study was approved by the NYIT's Institutional Review Board under protocol BHT-1290, and all subjects provided informed consent. Subjects were provided with an iPhone XR [49] running a custom data collection app designed to present common interaction modalities, such as swiping and tapping on the default virtual keyboard. The swiping task consisted of swiping a word, such as "Green", to the corresponding color on an edge of the phone. The color of the font was intentionally different from the color indicated by the word itself, requiring the user to engage in a simple cognitive task (see Figure 1). There were four colors in total, one on each edge of the screen. During all experiments, the smartphone's onboard sensors captured accelerometer, gyroscope, and swipe metrics along with the x and y pixel coordinates for each swipe and tap event.

To acquire precise body movement and posture information, we performed all experiments at NYIT's 3D motion capture studio, which is equipped with a 30-camera Vicon Nexus 2.6 Optical Motion continuous capture system. Subjects were instrumented with 39 reflective markers according to the Vicon Nexus Plug-In-Gait model [50], which places markers over the entire body including limbs, trunk, pelvis, and head. We customized the model by adding a marker to the base of the nail bed of each thumb. We also placed 3 markers, one mark each on the top, left, and right sides of the smartphone. The markers acted as discrete sensors of positions in space. 3D positional data of each marker was captured in the x, y, and z coordinates at 100 frames per second.

The 3D motion capture software used a Butterworth [51] filter to reduce noise. We relied on custom gap filling pipelines

[1] We planned to use data from 40 subjects in our experiments. However, for one subject, a motion capture sensor failed to record data in the second session. As a result, in this work we used 39 subjects in our experiments.

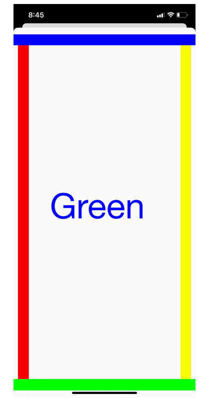

Fig. 1. Swiping task. The user must swipe the word "Green", presented in blue color font, to overlap with the green banner at the bottom of the screen.

from Vicon Nexus to determine sensor position during short periods when markers were not visible to the IR cameras. During data collection, users were asked to either walk around a square perimeter with sides of approximately 6 meters or sit on a chair without arm rests.

For each subject, data collection trials were divided in two sessions, spaced by about one-week on average. (Three users, which are not accounted for in this average, performed their session several months apart due to restrictions associated with COVID-19.) Sessions were divided in 24 sixty-second trials evenly split across 4 body posture/activity combinations, i.e., sit and swipe, sit and type, walk and swipe, walk and type. We randomized the order of the aforementioned combinations at the start of each session. We recorded a total of 29,827 swipes, defined as a continuous touchscreen interaction with a length of at least 35 pixels. All first sessions combined resulted in 14,190 swipes, while the second sessions resulted in 15,637 swipes. On average, each user performed 373 swipes per session, with a minimum of 192 and a maximum of 494 swipes. Smartphone and 3D motion capture data collected during the first session was used to construct the training sets for our authentication experiments. Data collected during the second session was used as genuine and impostor (test) data.

IV. Results

In our experiments, we used a set of 46 smartphone features based on swipe characteristics, captured by the smartphone's touchscreen, and phone-movement data, captured by the smartphone's accelerometer and gyroscope sensors (see Table II). We extracted a total of 83 features from 3D motion capture data, representing the user's posture and body movement based on distances, accelerations, and velocities of the motion capture markers, as well as angle-based relative direction features. Among the 83 features, 36 were excluded from our analysis due to their relatively low mutual information compared to other features. The 36 features excluded were the velocities and accelerations of hand, wrist, and elbow markers (on both the left and right arm), each of these 12 markers providing x, y, z dimensions of data. The resulting mutual information of all features used in our authentication experiments are presented in the Appendix (see tables VII

TABLE I
SELECTED RESEARCH RELATED TO BIOMETRIC AUTHENTICATION LEVERAGING SMARTPHONE BEHAVIORS AND BODY MOVEMENT. "PUBLIC" INDICATES THAT THE DATASET USED IN THE PAPER IS PUBLICLY AVAILABLE.

Work	# of users	Behaviors	Feature Extraction	Classifier(s)	Auth. Results
Munsell et al. (2012) [41]	10	Body movement while walking and running	100 videos captured with Kinect RGBD	SVM	13% EER
Derlatka et al. (2015) [43]	31	Body movement while walking and running	600 Gait cycles captured with Kistlers force plates, Kinect device, accelerometers	KNN	0.85% FAR 4.55% FRR 13% EER
Javid et al. (2016) [44]	60	Hand and body movement	Features captured from accelerometer, gyroscope	MLP, KNN, SVM, NB	81% - 97% accuracy
Kumar et al. (2016) [45]	28	Swiping, typing, phone movement while web browsing	Features captured with gyroscope	KNN, RF	93.33% accuracy
Shen et al. (2016) [5]	71	Swiping	Pressure, length, duration, angle, position, velocity	KNN, SVM BPNN, RF	8.87% EER
Sitova et al. (2016) [22]	100 (Public [22])	Hand movement, tapping while walking and sitting	60 resistance, 36 stability features captured with accelerometer, gyroscope, magnetometer	OSVM	7.16% EER
Balazia et al. (2017) [38]	48 (Public [46])	Body movement while walking	3D body joint coordinates captured with MoCap	1-NN	EER: 16.74%
Muhammad et al. (2017) [42]	35	Body movement with Smartphone	Gait data captured with accelerometer	Gait cycle estimation	13% EER
Li et al. (2018) [27]	100 (Public [22])	Hand and body movement	Feature captured with accelerometer, gyroscope	OSVM	8.33% overall EER (4.66% median EER)
Shen et al. (2018) [26]	102	Swiping and tapping while walking and sitting	Features captured with accelerometer, gyroscope, magnetometer, orientation	HMM-based	5.03% FRR 3.98% FAR
Garbuz et al. (2019) [2]	36	Swiping and tapping	Movement coordinates, timestamps captured with accelerometer, gyroscope, magnetometer	OSVM	Best FRR: 5% Best FAR: 7.1%
Kwolek et al. (2019) [39]	32 (Public [39])	Body movement while walking	Gait features captured with MoCap	NB, SVM, MLP, KNN 1,3,5-NN	Best CCR (accuracy) 94.83% with MLP
Volaka et al. (2019) [47]	100 (Public [22])	Scrolling, tapping while walking and sitting	Features captured with accelerometer, gyroscope, magnetometer	Binary Classification Neural Network	15% EER
Abuhamad et al. (2020) [48]	84	Swiping, typing, phone movement during normal user use	Feature captured with accelerometer, gyroscope, magnetometer, elevation	LSTM-based (RNN)	98% F1 Score 0.95% FAR 6.67% FRR 0.41% ERR
Ray-Dowling et al. (2022) [28]	100 [22] and 115 [29] (both public)	Swiping and typing while sitting	Features captured with accelerometer, gyroscope, magnetometer,	OSVM, Binary-SVM	1.5% and 0.2% EER
Chao et al. (2023) [3]	36	Swiping	Pressure, size, time, coordinate, velocity, hybrid captured with accelerometer, gyroscope, magnetometer, linear acceleration, gravity	SVM, RF	13.5%EER (right thumb) 8.1%EER (left thumb)
This Work (2024)	39 (Public)	Swiping, body movement while walking, sitting	46 smartphone swipe, accelerometer, gyroscope features, 47 features captured with 3D MoCap	SM, KNN RF, OSVM	5.35% EER with Random Forest at 5 seconds

and VIII for sitting and walking, respectively). The 47 motion capture features we retained for our authentication experiments are presented in Table III. These represent the user's posture and body movement in terms of distances, accelerations, and velocities of the motion capture markers. The angle-based features represent the azimuth angle θ, i.e., the angle of rotation from the meridian plane, and φ represents the angle with respect to the polar axis. Figure 2 provides a visual representation of θ and φ. Our features do not consider the radial distance r.

In our experiments, we focused the performance of each class of features as a function of the authentication latency, i.e., the time needed to collect enough data to trigger an authentication decision. In general, shorter authentication latencies are preferred because they allow the authentication system to identify the impostor more quickly, and therefore they tend to limit the amount of time available to the impostor to attack the system. For each class of features we report performance over very short (1 to 3 seconds), short (5 to 10 seconds) and long (15 to 60 seconds) authentication latencies. Our analysis separates results by body posture (sitting and walking), and body regions (upper, lower, and center).

In our analysis, we grouped the motion capture markers (and the features extracted from them) into *upper*, *center*, and *lower* body regions. The Vicon 3D Motion Capture system which we used to collect body motion data uses a full body Plug-In-Gait biomechanical model [50], which is a skeletal model representing the human body as a series of segments (skeleton) connected by joints. In the Vicon Plug-In-Gait model, there are a total of 10 segments, involving head, thorax, upper arm, forearm, hand, pelvis, hip, and knee. While such fine-grained segmentation of the skeletal model may be suitable for certain biomechanical studies ([52], [53]), we opted for a simpler model (upper, center, and lower), to aid the description

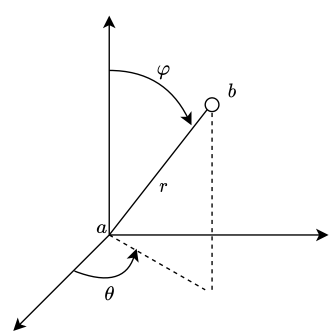

Fig. 2. Spherical coordinate system used for our relative-direction features. a and b represent two markers; φ represents the angle of rotation with respect to the polar axis, while θ is the azimuth angle.

TABLE II
SMARTPHONE SWIPE-BASED ("BASELINE") FEATURES.

Type	Feature	Description	# of dim.
Swipe Characteristics	Length	Total Length of Swipe	1
	Time	Time Duration of Swipe	1
	Angle	Angular Sum of Swipe	1
	Velocity	Average Velocity of Swipe	1
Accelerometer Data	Mean	Mean of Accelerometer Data in *x, y, z*	3
	SD	Standard Deviation of Accelerometer Data in *x, y, z*	3
	Kurtosis	Kurtosis of Accelerometer Data in *x, y, z*	3
	Max	Maximum of Accelerometer Data in *x, y, z*	3
	Min	Minimum of Accelerometer Data in *x, y, z*	3
	Energy	Energy of Accelerometer Data in *x, y, z*	3
	Entropy	Entropy of Accelerometer Data in *x, y, z*	3
Gyroscope Data	Mean	Mean of Gyroscope Data in *x, y, z*	3
	SD	Standard Deviation of Gyroscope Data in *x, y, z*	3
	Kurtosis	Kurtosis of Gyroscope Data in *x, y, z*	3
	Max	Maximum of Gyroscope Data in *x, y, z*	3
	Min	Minimum of Gyroscope Data in *x, y, z*	3
	Energy	Energy of Gyroscope Data in *x, y, z*	3
	Entropy	Entropy of Gyroscope Data in *x, y, z*	3
		Total Number of Features	**46**

TABLE III
3D MOTION CAPTURE DISTANCE, MOVEMENT, AND ANGLE FEATURES.

Type	Region	Feature	How the feature is calculated	# of dim.
Posture	Upper	Head-to-Phone Distance	Distance from the forehead to the phone marker	1
		Clavicle-to-Phone Distance	Distance from the clavicle marker to the phone marker	1
		Shoulders-to-Phone Distance	Distances from left and right shoulder markers to the phone marker	2
		Head-Phone Angles	Angles of the forehead to phone (attention) vector	2
		Neck to forehead Angles	Angles of the neck	2
		Shoulder to elbow Angles	Angles of the shoulders (arms)	4
	Center	Upper Spine	Angles of the upper (half of) spine	2
		Lower Spine	Angles of the lower (half of) spine	2
		Sternum-to-Phone Distance	Distance from the sternum marker to the phone	1
		Clavicle-to-Elbows Distance	Distance from the clavicle marker to either elbow	2
		Sternum-to-Elbows Distance	Distance from the sternum marker to either elbow	2
		Elbow to wrist Angles	Angles of the elbows	4
		Forearm to wrist Angles	Angles of the wrists	4
Body Movement	Lower	Hip-to-Phone Distance	Distance from either hip marker to the phone	2
		Hip-to-Elbows Distance	Distance from either hip marker to either elbow	4
		Hip Angles	Angles of the hips (legs)	4
		Knee Angles	Angles of the knees	4
		Ankle Angles	Angles of the ankles	4
			Total Number of Features	**47**

of our authentication results, and which broadly aligns with the task parameters of handling a smartphone. This practice is in alignment with current biomechanics standards, where studies use few or as many segments as needed to address their research problems (e.g., [54], [55], [53]).

We matched the user templates against the authentication (test) vectors using four methods: two one-class methods (Scaled Manhattan Distance (SM) [56] and One-Class Support Vector Machine (OSVM) [57]), and two two-class methods (Random Forest [58] (RF) and K-Nearest Neighbor (KNN) [59]). We chose these methods because they were among the most popular in the behavioral biometric literature (see [60], [28], and Table I) and because they represent diversity in their approaches to biometric matching: SM is distance-based; OSVM builds a "region" enclosing the target data points; RF represents both ensemble and induction learning paradigms; and KNN represents the neighbor-based approach. Further, RF and KNN represent supervised, and SM and OSVM represent semi-supervised biometric authentication.

To implement SM, we used the approach followed in [9]. We used the scikit-learn [61] implementations of OSVM, RF, and KNN. Each method was implemented in the verifier mode (i.e., each user has her own trained model). For training the two-class methods, we used the genuine examples in Session 1 and paired them with the impostor examples from 5 randomly-chosen impostors, who were then excluded from the test set. The parameter search and the preprocessing RF, KNN, and OSVM were done as follows. For RF, we performed a grid search over the "number of trees" (100 to 1000, in increments of 100), and the "maximum features" (2, 3 , and 4) parameters. For KNN, we searched over the "number of neighbors" parameter (2, 3, 4, 5). OSVM is sensitive to outliers [62], and therefore we implemented outlier filtering with Isolation Forest [63] (10% contamination) and reduced the dimensionality of the feature set with Principal Component Analysis (PCA) [64]. We then conducted a grid-search with the ν parameter set to 0.05, 0.1, 0.2, and 0.3, the γ parameter set to 0.001, 0.01, 0.1, and "*scale*", and the number of PCA components set to 2, 3, 4, and 5.[2] We report the error rates achieved from the best performing parameter values.[3] To get the scores, we used the `predict_proba` function for RF

[2]Before fixing the limits for the grid search, we experimented with high values of γ, which did not perform well.

[3]The grid search was conducted to optimize HTER error metric.

and KNN, and the `decision_function` for OSVM.

A. Biometric Viability of Posture and Body Movement Features

Table IV shows the EERs of the touchscreen and phone movement features listed in Table II. In the rest of the paper, we refer to these features as *baseline features*. The same table also shows the EERs of body movement features (upper, center, and lower body features, listed in Table III) for both walking and sitting postures. Our results show that posture and body movement features consistently outperform baseline features with very short (1- to 3-second) and short (5- and 10-second) authentication windows, across both body postures, and regardless of the body region. In particular, we saw a consistent reduction in the EERs of the posture and body movement features in comparison to the baseline features as the authentication window length decreased, indicating that the posture and body movement features are very well-suited at capturing distinctive user characteristics within very short and short authentication windows.

B. Feature-level Fusion of Baseline Features with Posture and Body Movement Features

Our results show that fusing all three regions' posture and body movement features with the baseline features yields the lowest EERs by a significant margin. The error reduction is evident as shown in Figure 3. For very short authentication windows, fusing features from all regions with baseline features outperformed baseline features alone. This was the case for both sitting and walking, and for all verification methods used in our evaluation.

For all other authentication windows, fusing features from all the regions with the baseline again outperformed baseline features alone in both sitting and walking postures for three of the verification methods: SM, RF, and KNN. With OSVM we observed a relatively smaller reductions in EERs for walking. Further, the EERs of OSVM increased as the authentication window size increased for sitting (see Figure 3). We believe that this behavior can be attributed to the low training sample size. OSVMs are sensitive to low density of the target class samples, which can drastically alter the "support" on which the boundary is constructed, and deteriorate generalization [65], [62]. In our case, as the authentication window size increased, the number of genuine samples available for training decreased, thus impacting OSVM's ability to generalize.

Finally, our fusion results in Figure 3 show that RF performs best for short and very short authentication windows in both sitting and walking, followed by SM. This indicates that feature-level fusion can additionally benefit from using an appropriate verification method (e.g., supervised vs. semi-supervised), which is also consistent from the results reported in benchmarking studies in behavioral biometrics where some methods tend to outperform others (e.g., see [60], [6], [26]).

Table V highlights the contributions of features from each individual region when they are fused with baseline features. To this end, the table shows the *reduction* in EERs achieved by fusing the baseline features with the posture and body movement features, as compared to baseline features alone (positive numbers represent a decrease in EER). For very short authentication windows, fusing features from all regions with baseline features outperformed baseline features alone in each of the individual regions. Similarly, for all remaining authentication windows, including the short authentication windows, fusing features from all regions with the baseline features outperformed baseline features fused with any of the individual regions. This observation is true for SM, RF, and KNN verifiers for walking.

OSVM continued to show sensitivity to the training sample size. As the authentication window sizes increased, the feature-level fusion performance decreased for both sitting and walking. In fact, in some instances OSVM was forced to use a lower number of principal components due to the sample size. We indicate these instances with "*" in tables IV and V. For short authentication windows and above in the sitting posture, fusion of features from all regions with baseline outperformed individual regions for SM and RF methods, while features of lower region fused with baseline performed slightly better with OSVM and KNN.

In summary, our results indicate the following general trends, especially in the context of lowering error rates for very short and short authentication windows: (1) posture and body movement features collected across the body contribute to achieving the lowest EERs with very short and short authentication windows; and (2) reductions in error rates can also be achieved by using posture and body movement features collected from individual body regions, albeit not at the same level as with features from all regions.

C. Determining the Impact of Anthropometric Characteristics on Posture and Body Movement Features

A body-static feature is loosely defined as a feature with a significant component determined by the user's anthropometric (physiological) characteristics. For example, the arm length is completely body-static, whereas elbow joint angle is not, even though there might be a dependency between the latter and the former. Under the assumption that anthropometric characteristics carry biometric information, we evaluated the degree of dependency between strictly behavioral features and anthropometric characteristics. Specifically, we determined whether the gain in mutual information from a particular behavioral feature is dominated by some underlying body-static component. To do so, we scaled each feature by the distance between the elbow and the wrist, which is an anthropometric feature. We then compared the mutual information of the scaled feature with that of the original feature. For example, when the feature sternum to left elbow distance was scaled by the *wrist to elbow* distance mutual information was reduced by 9.84%. These changes are presented in Table VI. If the mutual information of the scaled feature is lower than that of the original feature, then we concluded that the original feature had a body-static component.

Table VI shows the features with the largest relative reduction in mutual information after the scaling while users were sitting and walking. We used this ranking to determine

TABLE IV
EERS FOR BASELINE DATA AND MOTION CAPTURE DATA FOR EACH REGION, SPLIT BY BODY MOTION TYPE FOR EACH CLASSIFIERS.

Method	**Posture**	**Feature Set**	**Window Length in Seconds**								
			1	**2**	**3**	**5**	**10**	**15**	**20**	**30**	**60**
SM	Walk	Baseline Only	0.395	0.328	0.286	0.237	0.183	0.163	0.150	0.135	0.096
		Upper Region Only	0.252	0.199	0.191	0.181	0.177	0.175	0.178	0.174	0.155
		Center Region Only	0.228	0.154	0.142	0.127	0.120	0.119	0.120	0.117	0.108
		Lower Region Only	0.261	0.199	0.190	0.179	0.174	0.167	0.168	0.168	0.155
	Sit	Baseline Only	0.331	0.263	0.230	0.193	0.162	0.150	0.137	0.127	0.117
		Upper Region Only	0.223	0.179	0.169	0.157	0.157	0.158	0.158	0.153	0.168
		Center Region Only	0.220	0.163	0.149	0.135	0.134	0.133	0.134	0.131	0.127
		Lower Region Only	0.220	0.166	0.150	0.135	0.134	0.134	0.135	0.132	0.135
OSVM	Walk	Baseline Only	0.368	0.317	0.296	0.258	0.238	0.213	0.219	0.191	0.183
		Upper Region Only	0.233	0.230	0.230	0.236	0.234	0.231	0.237	0.239	0.210
		Center Region Only	0.185	0.183	0.185	0.182	0.183	0.184	0.176	0.178	0.173
		Lower Region Only	0.238	0.218	0.220	0.220	0.232	0.227	0.232	0.230	0.233
	Sit	Baseline Only	0.286	0.259	0.242	0.217	0.204	0.177	0.185	0.169	0.156
		Upper Region Only	0.243	0.239	0.220	0.224	0.226	0.218	0.225	0.211	0.220
		Center Region Only	0.221	0.221	0.224	0.234	0.222	0.230	0.237	0.235	*0.250
		Lower Region Only	0.162	0.162	0.162	0.162	0.162	0.163	0.163	0.159	*0.206
RF	Walk	Baseline Only	0.233	0.210	0.213	0.192	0.156	0.158	0.144	0.160	0.157
		Upper Region Only	0.164	0.165	0.152	0.165	0.169	0.174	0.189	0.180	0.172
		Center Region Only	0.111	0.116	0.132	0.100	0.120	0.140	0.125	0.140	0.145
		Lower Region Only	0.153	0.168	0.167	0.165	0.173	0.166	0.165	0.187	0.208
	Sit	Baseline Only	0.194	0.185	0.182	0.187	0.165	0.164	0.157	0.161	0.146
		Upper Region Only	0.137	0.135	0.131	0.139	0.144	0.162	0.155	0.138	0.145
		Center Region Only	0.099	0.089	0.151	0.124	0.107	0.099	0.105	0.110	0.130
		Lower Region Only	0.150	0.169	0.169	0.170	0.159	0.149	0.180	0.181	0.153
KNN	Walk	Baseline Only	0.408	0.399	0.394	0.372	0.363	0.341	0.363	0.334	0.349
		Upper Region Only	0.274	0.297	0.271	0.267	0.256	0.267	0.278	0.276	0.293
		Center Region Only	0.284	0.287	0.255	0.287	0.244	0.258	0.239	0.259	0.277
		Lower Region Only	0.268	0.270	0.271	0.276	0.243	0.238	0.235	0.248	0.258
	Sit	Baseline Only	0.392	0.390	0.387	0.380	0.357	0.374	0.349	0.359	0.333
		Upper Region Only	0.278	0.279	0.253	0.265	0.235	0.241	0.255	0.259	0.260
		Center Region Only	0.282	0.283	0.297	0.277	0.256	0.274	0.293	0.281	0.286
		Lower Region Only	0.228	0.254	0.242	0.243	0.251	0.187	0.202	0.230	0.172

TABLE V
DECREASE IN EERS BETWEEN BASELINE FEATURES AND FEATURE-LEVEL FUSION OF BASELINE WITH POSTURE AND BODY MOVEMENT FEATURES USING VARYING CLASSIFIERS. POSITIVE NUMBERS INDICATE A DECREMENT OF EER COMPARED TO THE BASELINE.

Method	**Posture**	**Feature-level Fusion**	**Window Length in Seconds**								
			1	**2**	**3**	**5**	**10**	**15**	**20**	**30**	**60**
SM	Walk	Upper Region + Baseline	0.124	0.126	0.112	0.092	0.064	0.053	0.044	0.037	0.016
		Center Region + Baseline	0.161	0.170	0.147	0.123	0.087	0.077	0.066	0.049	0.023
		Lower Region + Baseline	0.124	0.130	0.113	0.091	0.059	0.043	0.038	0.037	0.022
		All Regions + Baseline	0.180	0.190	0.165	0.136	0.091	0.076	0.066	0.052	0.022
	Sit	Upper Region + Baseline	0.096	0.082	0.067	0.045	0.025	0.017	0.009	0.004	0.001
		Center Region + Baseline	0.106	0.097	0.083	0.065	0.043	0.036	0.025	0.019	0.016
		Lower Region + Baseline	0.120	0.110	0.094	0.073	0.049	0.041	0.029	0.024	0.019
		All Regions + Baseline	0.133	0.128	0.113	0.094	0.066	0.055	0.043	0.036	0.033
OSVM	Walk	Upper Region + Baseline	0.073	0.039	0.029	0.012	0.005	0.013	0.008	-0.011	0.003
		Center Region + Baseline	0.122	0.084	0.073	0.053	0.044	0.024	0.024	0.024	0.027
		Lower Region + Baseline	0.084	0.042	0.044	0.012	0.034	0.032	0.023	0.005	0.026
		All Regions + Baseline	0.129	0.091	0.064	0.043	0.023	0.005	0.014	0.014	0.026
	Sit	Upper Region + Baseline	0.021	0.009	0.001	-0.006	-0.001	-0.033	-0.029	-0.029	-0.064
		Center Region + Baseline	0.040	0.020	0.004	-0.013	-0.011	-0.045	-0.028	-0.030	*-0.104
		Lower Region + Baseline	0.062	0.050	0.056	0.041	0.018	-0.003	0.013	0.006	*-0.056
		All Regions + Baseline	0.050	0.030	0.019	-0.010	-0.014	-0.039	-0.027	-0.025	*-0.082
RF	Walk	Upper Region + Baseline	0.101	0.089	0.083	0.079	0.016	0.036	0.032	0.031	0.043
		Center Region + Baseline	0.135	0.117	0.123	0.096	0.073	0.080	0.041	0.058	0.058
		Lower Region + Baseline	0.097	0.093	0.086	0.082	0.041	0.047	0.037	0.042	0.028
		All Regions + Baseline	0.169	0.134	0.154	0.123	0.081	0.089	0.062	0.083	0.077
	Sit	Upper Region + Baseline	0.095	0.074	0.079	0.086	0.056	0.040	0.045	0.037	0.033
		Center Region + Baseline	0.122	0.116	0.106	0.106	0.066	0.065	0.063	0.064	0.025
		Lower Region + Baseline	0.067	0.083	0.082	0.089	0.066	0.081	0.055	0.054	0.053
		All Regions + Baseline	0.120	0.116	0.127	0.134	0.101	0.098	0.090	0.085	0.058
KNN	Walk	Upper Region + Baseline	0.140	0.139	0.145	0.130	0.116	0.107	0.107	0.073	0.091
		Center Region + Baseline	0.137	0.151	0.126	0.100	0.103	0.094	0.123	0.094	0.097
		Lower Region + Baseline	0.145	0.154	0.140	0.137	0.123	0.111	0.133	0.101	0.112
		All Regions + Baseline	0.149	0.160	0.149	0.142	0.123	0.113	0.148	0.114	0.097
	Sit	Upper Region + Baseline	0.146	0.158	0.144	0.136	0.119	0.140	0.141	0.136	0.092
		Center Region + Baseline	0.105	0.099	0.117	0.113	0.083	0.131	0.066	0.098	0.059
		Lower Region + Baseline	0.182	0.186	0.187	0.184	0.150	0.207	0.187	0.170	0.164
		All Regions + Baseline	0.138	0.152	0.158	0.134	0.134	0.174	0.154	0.138	0.145

feature exclusion criteria for features dominated by body-static components. By selecting features with low body-static components, our analysis can focus on features that are more likely to be inherently behavioral. The features exhibiting the greatest reduction in mutual information were partitioned into three distinct groups: the first group *excluded* the top 33% of features (rows 1–4 for sitting, and rows 14–20 for walking in Table VI) characterized by the highest loss in mutual informa-

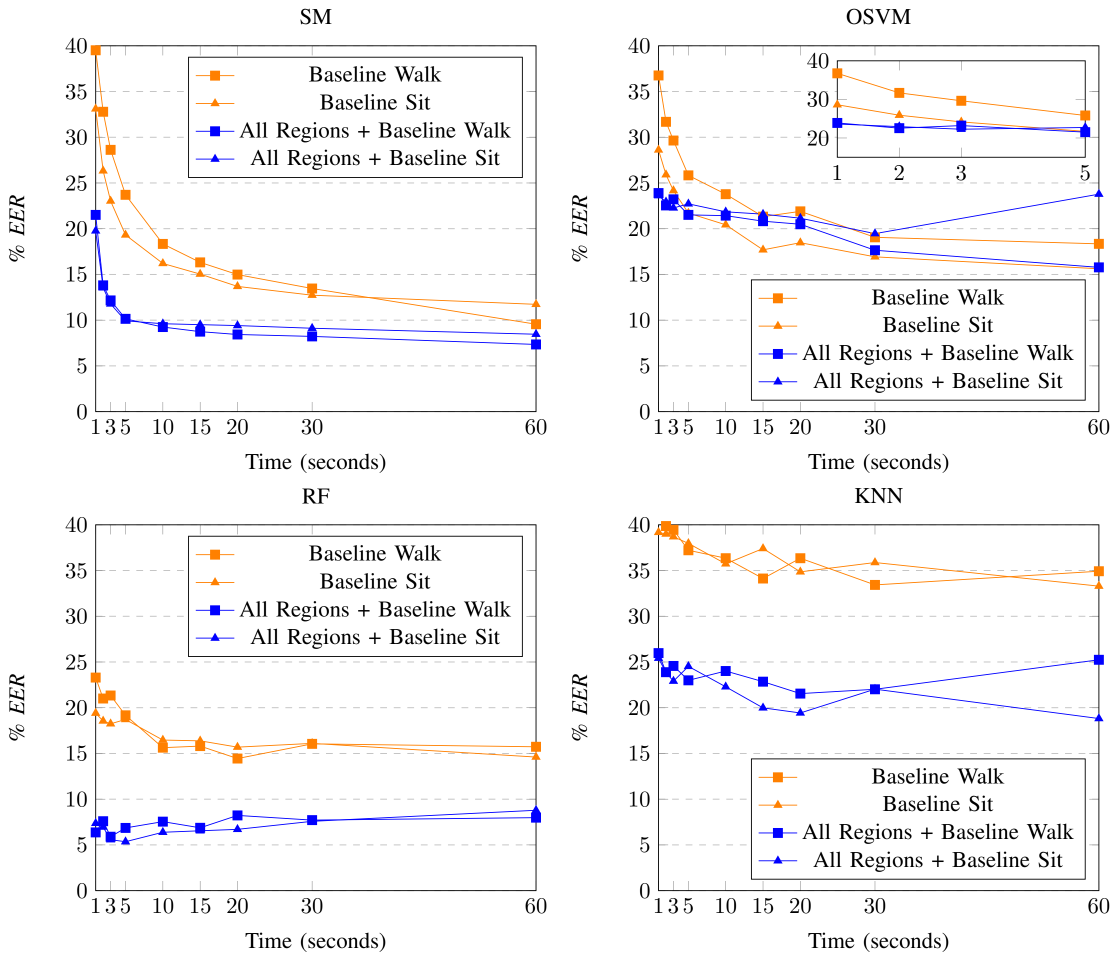

Fig. 3. EERs of baseline features vs. feature-level fusion of posture and body movement features from all regions in sit and walk conditions for each verifier.

tion; the second group excluded the top 66% of features (rows 1–8 for sitting, and rows 14–27 for walking in Table VI with the highest loss; and the third group encompassed none of the features listed in Table VI for sitting and walking. Figure 4 and Figure 5 show the resulting EERs with and without the excluded features for walking and sitting for each verifier.

For walking, we achieved the lowest EERs when using all features with very short and short authentication windows (see Figure 4). Notably, this was also the case with 33%-, 66%-, 100%-exclusion feature sets, indicating that the behavioral aspects of posture and body movement features, when fused with baseline features, can achieve error rates that are better than the baseline features alone. However, this advantage gradually dissipated as the authentication window sizes increased (e.g., at 60s). With OSVM in particular, the elimination of body-static features along with reduction of training sample sizes caused a significant deterioration of our fusion results.

For sitting, we achieved the lowest EERs when using all features with very short and short authentication windows (see Figure 5). As with walking, this was the case with 33%-, 66%-, 100%-exclusion feature sets, again indicating that the behavioral aspects of posture and body movement features, when fused with baseline features, can achieve error rates that are better than baseline features alone. As with walking, OSVM results deteriorated for longer authentication windows.

V. Capturing Posture and Body Movement with Smartphones and Wearable Devices

The results presented in this paper demonstrate that it is possible to reliably authenticate users within very short authentication windows when smartphone behavioral features are augmented with posture and body movement features. However, deploying an external 3D motion capture system with body markers for the purpose of continuous authentication is clearly impractical. To close this gap, in this section we discuss how recent work in the area of body tracking using smartphones and wearable devices can be leveraged to acquire the posture and body movement features used in this work.

Liang et al. [66] introduce Pano+Track, a persistent authentication model that uses hand and body tracking to verify whether the user continues to have "custody" of their smartphone. Pano+Track uses a fisheye camera mounted on the smartphone to capture both near-field information (to perform hand gesture tracking), and full-scene information (to perform body tracking). For body tracking, [66] implements body keypoint prediction and skeleton estimation, and extracts three body features: head orientation, head-to-camera distance, and body-hand-phone connectivity. Pano+Track achieves 81.6%

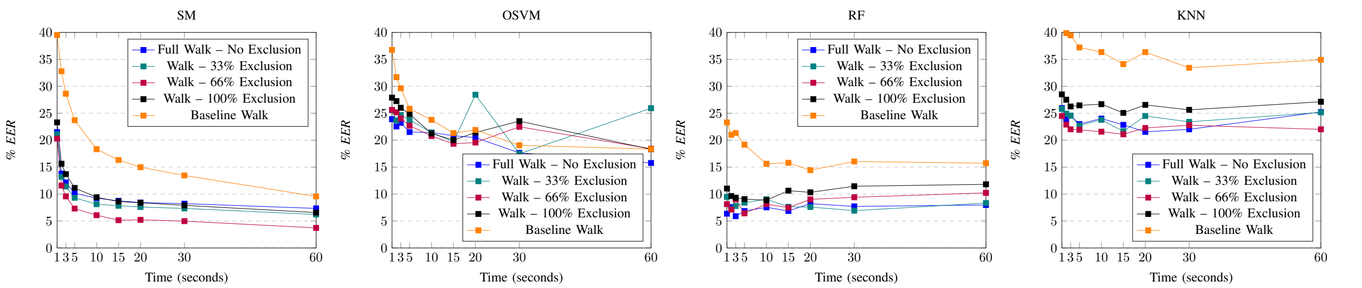

Fig. 4. Feature-level fusion results with each classifier for 33%-, 66%-, and 100%-exclusion features sets (Table VI) as compared to no exclusion, and the baseline for walking posture.

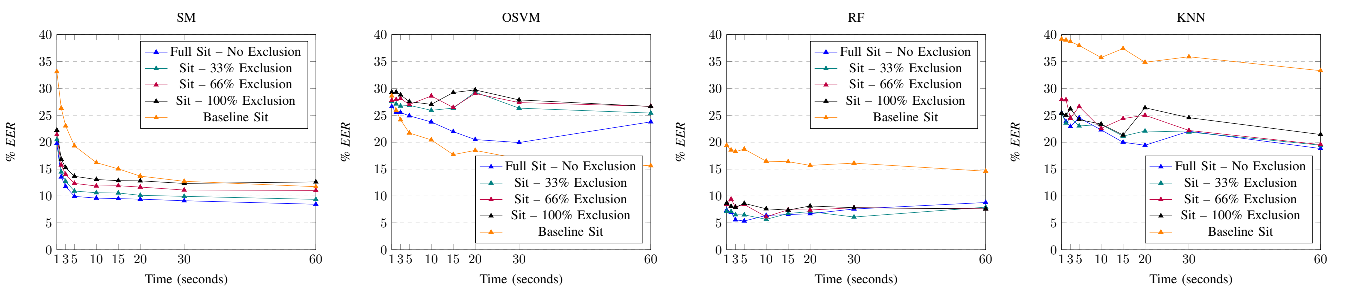

Fig. 5. Feature-level fusion results with each verifier for 33%-, 66%-, and 100%-exclusion features sets (Table VI) as compared to no exclusion, and the baseline for sitting posture.

TABLE VI
EXCLUSION CRITERIA BY % CHANGE IN MUTUAL INFORMATION (MI) OF POSTURE AND BODY MOVEMENT FEATURES. A NEGATIVE SIGN INDICATES DECREASE IN MI AFTER CORRECTING FOR A BODY-STATIC COMPONENT.

Sitting		
ID	**Feature**	**% Change in MI**
1	Clavicle to Right Elbow distance	-21.402
2	Clavicle to Left Elbow distance	-13.460
3	Sternum to Right Elbow distance	-10.615
4	Sternum to Left Elbow distance	-9.841
5	Right Hip to Left Elbow distance	-5.579
6	Left Hip to Left Elbow distance	-4.546
7	Left Shoulder to Phone distance	-4.410
8	Left Hip to Right Elbow distance	-4.319
9	Right Hip to Right Elbow distance	-3.588
10	Right Elbow θ Angle	-2.576
11	Right Shoulder to Phone distance	-2.566
12	Upper Spine ϕ Angle	-0.806
13	Left Shoulder θ Angle	-0.162
Walking		
14	Right Hip to Right Elbow distance	-51.005
15	Right Knee ϕ Angle	-48.096
16	Left Elbow ϕ Angle	-43.298
17	Left Knee ϕ Angle	-43.069
18	Head to Phone θ Angle	-41.741
19	Right Elbow θ Angle	-41.598
20	Left Wrist θ Angle	-40.973
21	Upper Spine θ Angle	-39.883
22	Right Ankle θ Angle	-39.882
23	Left Ankle θ Angle	-38.127
24	Neck θ Angle	-28.826
25	Clavicle to Right Elbow distance	-28.021
26	Left Elbow θ Angle	-27.419
27	Clavicle to Left Elbow distance	-24.692
28	Sternum to Right Elbow distance	-24.618
29	Left Hip to Right Elbow distance	-20.474
30	Left Hip to Phone distance	-19.108
31	Sternum to Left Elbow distance	-18.533
32	Right Hip to Left Elbow distance	-17.444
33	Sternum to Phone distance	-9.751
34	Right Hip to Phone distance	-5.013

and 99.4% accuracies for body detection at approximately 4m and less than 1m distances respectively, and an accuracy of 97.5% for hand gesture detection. Pano+Track also achieves 94.3% persistent authentication accuracy with 14 subjects, with face biometric used as the initial point of authentication.

Ahuja et al. [67] propose "Pose-on-the-Go", a full body continuous pose estimation system that uses only smartphone sensors and no additional hardware. This system performs fusion of data from the smartphone's front and rear cameras, IMU sensors, and touchscreen, and utilizes inverse kinematics (IK) SDK to estimate body tracking and pose data such as "angle of the elbow joint", "head orientation and position relative to the phone", "torso orientation", "arm pose", and leg and locomotion poses. Ahuja et al. [67] also report the accuracy of their pose estimation. Their system was able to achieve a mean angular error of 6.4° head orientation (yaw, pitch, and roll), 26.1° for torso pose estimation, and a mean spatial euclidean error of 18cm across three joints (wrist, shoulder, and elbow). Further, [67] also report the angular wrist joint errors as 11.5, 9.1, and 8.9 degrees for yaw, pitch, and roll respectively. Ahuja et al. [67] conclude that their system, though achieves a coarse grained full body pose estimation, is welcome first step towards achieving smartphone-based full body tracking without adding any additional hardware to the smartphone.

Kim et al. [68] propose OddEyeCam, a vision-based smartphone system that tracks user's body in space. To this end, OddEyeCam continuously captures RGB images using a low-resolution wide-angle (180°) camera, and depth information using a narrow-field depth-sensing camera, both of which are mounted on top of the smartphone's screen. This data is fused with the built-in smartphone accelerometer. Kim et al. evaluated OddEyeCam with data from 10 subjects and showed that it can effectively track body landmarks within the field of view of the RGB camera with an average estimation error of 4.3cm. Given that popular smartphones already integrate both a 3D depth sensors and a high-resolution wide-angle front-facing cameras, we believe that OddEyeCam can be used to accurately extract the position of a number of landmarks used in this work with off-the-shelf smartphone hardware.

In [69], Tome et al. propose SelfPose, a system that uses a downward looking fisheye camera mounted on an VR headset to track body poses from an eco-centric perspective (i.e., the camera faces the camera-wearer). SelfPose employs a multi-branch deep encoder-decoder architecture that takes monocular images from the fisheye camera, estimates a heat map, and then uses an autoencoder-decoder to estimate body positions. The output of the system is the 3D positional points of the body joints. Further, SelfPose estimates joint rotations from positional information. Tome et al. [69] quantified SelfPose's performance in terms of mean per joint position error and reported the estimation errors in millimeter scale for head, hand, arm, elbow, knee, foot, and ankle joints (see Table 3 in [69]), and noted that higher errors occur in the hands and feet, which were the most occluded body regions with their ego-centric tracking system.

In addition to the work listed in this above, several studies demonstrate 3D full body pose tracking with smartphones [70], [71] and other wearable devices [72], [73], [74], [75], [76]. Further, there are many studies that perform partial body tracking such as hand, wrist, hip, and leg tracking (see, e.g., [77], [78], [79], [80]).

Combined, the studies presented in this section demonstrate that it is feasible to track a wide variety of postures and body movements using smartphones and wearable devices. Several of the sensors needed for tracking are either ubiquitous (e.g., front-facing camera and inertial sensors) or are available in many of high-end smartphones (e.g., depth sensors). Further, the remaining specialized sensors can be built with today's technology (e.g., [68], [69]), and have been shown to perform remarkably well in tracking postures and body movements. Because none of these systems are as accurate as 3D motion capture equipment, one interesting open question arises: to what extent do the errors introduced by smartphone- and wearable-based body tracking impact authentication error rates? We hope that the results presented in this paper will inspire future research to address this question.

VI. Conclusion

In this paper we demonstrate the benefits of incorporating posture and body movement features in continuous smartphone user authentication. Our findings indicate that these features can substantially enhance the accuracy of behavioral biometric systems, and reduce authentication latencies to 1–5 seconds. As a result, our features improve the security of continuous smartphone user authentication by stopping impostors within seconds, i.e., before they can successfully carry out an attack.

We achieved the lowest error rates by combining features from the upper, center, and lower regions of the user's body. Our results show that the EERs for touchscreen and movement-based features are significantly reduced when combined with body-motion features in both sitting and walking postures. For instance, while sitting, the EER was reduced to 5.4% for a 5-second authentication window, compared to an EER of 15.7% with a 60-second window when using swipe features only, with the two-class verifier (Random Forest). When the authentication window is further reduced to 1 second, our EER increased to just 6.4% which, remarkably, is still lower than what was achieved with 60-second baseline (swipe) features. For reference, using baseline features alone the EER was 23.3% for 1-second authentication latency. With the one-class verifier (Scaled Manhattan Distance), we achieved 11.8% EER for 3-second authentication window and 9.9% EER for 5-second window using our features, compared to 11.7% EER for 60-second window using baseline features alone.

References

[1] M. A. Shah and et al., "Continuous authentication in smartphones: An analysis on robust security practices," in *Future Technologies Conference (FTC) 2017*, Vancouver, November 2017.

[2] A. Garbuz, A. Epishkina, and K. Kogos, "Continuous authentication of smartphone users via swipes and taps analysis," in *2019 European Intelligence and Security Informatics Conf.*, Finland, 2019, pp. 48–53.

[3] J. Chao, M. S. Hossain, and L. Lancor, "Swipe gestures for user authentication in smartphones," *Journal of Information Security and Applications*, vol. 74, p. 103450, 2023.

[4] X. Zhao, T. Feng, W. Shi, and I. A. Kakadiaris, "Mobile user authentication using statistical touch dynamics images," *IEEE Transactions on Information Forensics and Security*, vol. 9, no. 11, pp. 1780–1789, 2014.

[5] C. Shen, Y. Zhang, X. Guan, and R. A. Maxion, "Performance analysis of touch-interaction behavior for active smartphone authentication," *IEEE Transactions on Information Forensics and Security*, vol. 11, no. 3, pp. 498–513, March 2016.

[6] J. Fierrez, A. Pozo, M. Martinez-Diaz, J. Galbally, and A. Morales, "Benchmarking touchscreen biometrics for mobile authentication," *IEEE Transactions on Information Forensics and Security*, vol. 13, no. 11, pp. 2720–2733, Nov 2018.

[7] M. Frank, R. Biedert, E. Ma, I. Martinovic, and D. Song, "Touchalytics: On the applicability of touchscreen input as a behavioral biometric for continuous authentication," *IEEE Transactions on Information Forensics and Security*, vol. 8, no. 1, pp. 136–148, Jan 2013.

[8] I. Lamiche, G. Bin, Y. Jing, and et al., "A continuous smartphone authentication method based on gait patterns and keystroke dynamics," *J Ambient Intell Human Comput*, vol. 10, pp. 4417–4430, 2019.

[9] K. S. Killourhy and R. A. Maxion, "Comparing anomaly-detection algorithms for keystroke dynamics," in *2009 IEEE/IFIP Intl. Conference on Dependable Systems & Networks*, Lisbon, 2009, pp. 125–134.

[10] T. Feng, X. Zhao, B. Carbunar, and W. Shi, "Continuous mobile authentication using virtual key typing biometrics," in *TRUSTCOM*, 2013.

[11] M. Trojahn and F. Ortmeier, "Biometric authentication through a virtual keyboard for smartphones," *International Journal of Computer Science & Information Technology*, vol. 4, no. 5, 2012.

[12] R. Kumar, V. V. Phoha, and R. Raina, "Authenticating users through their arm movement patterns," *arXiv preprint arXiv:1603.02211*, 2016.

[13] A. Primo, V. V. Phoha, R. Kumar, and A. Serwadda, "Context-aware active authentication using smartphone accelerometer measurements," in *Proceedings of the IEEE Conference on Computer Vision and Pattern Recognition Workshops*, 2014, p. 98–105.

[14] C. Bo, L. Zhang, X.-Y. Li, Q. Huang, and Y. Wang, "Silentsense: Silent user identification via touch and movement behavioral biometrics," in *MobiCom*, 2013.

[15] J. R. Kwapisz, G. M. Weiss, and S. A. Moore, "Activity recognition using cell phone accelerometers," *SIGKDD Explor. Newsl.*, vol. 12, no. 2, pp. 74–82, Mar. 2011.

[16] N. Khamsemanan, C. Nattee, and N. Jianwattanapaisarn, "Human identification from freestyle walks using posture-based gait feature," *IEEE Transactions on Information Forensics and Security*, vol. 13, no. 1, pp. 119–128, 2018.

[17] A. Bulling, U. Blanke, and B. Schiele, "A tutorial on human activity recognition using body-worn inertial sensors," *ACM Computing Surveys (CSUR)*, vol. 46, no. 3, p. 33, 2014.
[18] L. He, C. Ma, C. Tu, and Y. Zhang, "Gait2vec: Continuous authentication of smartphone users based on gait behavior," in *2022 IEEE 25th International Conference on Computer Supported Cooperative Work in Design (CSCWD)*, 2022, pp. 280–285.
[19] X. Huang, S. Nishimura, and B. Wu, "A pose detection based continuous authentication system design via gait feature analysis," in *2022 IEEE Intl Conf on Dependable, Autonomic and Secure Computing*, 2022, pp. 1–5.
[20] D. Crouse, H. Han, D. Chandra, B. Barbello, and A. K. Jain, "Continuous authentication of mobile user: Fusion of face image and inertial measurement unit data," in *2015 International Conference on Biometrics (ICB)*, May 2015, pp. 135–142.
[21] Y. Chen, T. Ni, W. Xu, and T. Gu, "Swipepass: Acoustic-based second-factor user authentication for smartphones," *Proc. ACM Interact. Mob. Wearable Ubiquitous Technol.*, vol. 6, no. 3, sep 2022.
[22] Z. Sitová, J. Šeděnka, Q. Yang, G. Peng, G. Zhou, P. Gasti, and K. S. Balagani, "Hmog: New behavioral biometric features for continuous authentication of smartphone users," *IEEE Transactions on Information Forensics and Security*, vol. 11, no. 5, pp. 877–892, May 2016.
[23] O. Banos, J.-M. Galvez, M. Damas, H. Pomares, and I. Rojas, "Window size impact in human activity recognition," *Sensors*, vol. 14, no. 4, pp. 6474–6499, 2014.
[24] A. Ray-Dowling, D. Hou, and S. Schuckers, "Stationary mobile behavioral biometrics: A survey," *Computers & Security*, vol. 128, p. 103184, 2023.
[25] M. Abuhamad, A. Abusnaina, D. H. Nyang, and D. Mohaisen, "Sensor-based continuous authentication of smartphones' users using behavioral biometrics: A contemporary survey," *IEEE IoT Journal*, 2020.
[26] C. Shen, Y. Li, Y. Chen, X. Guan, and R. A. Maxion, "Performance analysis of multi-motion sensor behavior for active smartphone authentication," *IEEE Transactions on Information Forensics and Security*, vol. 13, no. 1, pp. 48–62, Jan 2018.
[27] Y. Li, H. Hu, and G. Zhou, "Using data augmentation in continuous authentication on smartphones," *IEEE IoT Journal*, vol. 6, no. 1, pp. 628–640, Feb 2019.
[28] A. Ray-Dowling, D. Hou, S. Schuckers, and A. Barbir, "Evaluating multi-modal mobile behavioral biometrics using public datasets," *Computers & Security*, vol. 121, p. 102868, 2022.
[29] A. K. Belman, L. Wang, S. S. Iyengar, P. Sniatala, R. Wright, R. Dora, J. Baldwin, Z. Jin, and V. V. Phoha, "Insights from BB-MAS - A large dataset for typing, gait and swipes of the same person on desktop, tablet and phone," *CoRR*, vol. abs/1912.02736, 2019.
[30] M. M. Islam, S. Nooruddin, F. Karray, and G. Muhammad, "Multi-level feature fusion for multimodal human activity recognition in internet of healthcare things," *Information Fusion*, vol. 94, pp. 17–31, 2023.
[31] S. Mekruksavanich and A. Jitpattanakul, "Multimodal wearable sensing for sport-related activity recognition using deep learning networks," *Journal of Advances in Information Technology*, 2022.
[32] A. Reiss, G. Hendeby, and D. Stricker, "A competitive approach for human activity recognition on smartphones," in *European Symposium on Artificial Neural Networks, Computational Intelligence and Machine Learning, 24-26 April, Bruges, Belgium*. ESANN, 2013, pp. 455–460.
[33] O. D. Lara and M. A. Labrador, "A survey on human activity recognition using wearable sensors," *IEEE communications surveys & tutorials*, vol. 15, no. 3, pp. 1192–1209, 2013.
[34] J. Wu, P. Ishwar, and J. Konrad, "The value of posture, build and dynamics in gesture-based user authentication," in *IEEE International Joint Conference on Biometrics*, 2014, pp. 1–8.
[35] S. Dernbach, B. Das, N. C. Krishnan, B. L. Thomas, and D. J. Cook, "Simple and complex activity recognition through smart phones," in *2012 8th Intl. Conference on Intelligent Environments*, June 2012.
[36] I. Olade, C. Fleming, and H.-N. Liang, "Biomove: Biometric user identification from human kinesiological movements for virtual reality systems," *Sensors*, vol. 20, no. 10, 2020.
[37] A. Chatterjee, R. Fournier, A. Nait-Ali, and P. Siarry, "A postural information-based biometric authentication system employing s-transform, radial basis function network, and extended kalman filtering," *IEEE Transactions on Instrumentation and Measurement*, vol. 59, no. 12, pp. 3131–3138, 2010.
[38] M. Balazia and K. N. Plataniotis, "Human gait recognition from motion capture data in signature poses," *IET Biometrics*, vol. 6, no. 2, 2017.
[39] B. Kwolek, A. Michalczuk, T. Krzeszowski *et al.*, "Calibrated and synchronized multi-view video and motion capture dataset for evaluation of gait recognition," *Multimedia Tools and Applications*, vol. 78, pp. 32 437–32 465, 2019.
[40] R. Klempous, *Biometric Motion Identification Based on Motion Capture*. Berlin, Heidelberg: Springer Berlin Heidelberg, 2009, pp. 335–348.
[41] B. C. Munsell, A. Temlyakov, C. Qu, and S. Wang, "Person identification using full-body motion and anthropometric biometrics from kinect videos," in *Computer Vision – ECCV 2012. Workshops and Demonstrations*, Berlin, Heidelberg, 2012, pp. 91–100.
[42] M. Muaaz and R. Mayrhofer, "Smartphone-based gait recognition: From authentication to imitation," *IEEE Transactions on Mobile Computing*, vol. 16, no. 11, pp. 3209–3221, Nov 2017.
[43] M. Derlatka and M. Bogdan, "Fusion of static and dynamic parameters at decision level in human gait recognition," in *Pattern Recognition and Machine Intelligence*. Cham: Springer International Publishing, 2015, pp. 515–524.
[44] J. Maghsoudi and C. C. Tappert, "A behavioral biometrics user authentication study using motion data from android smartphones," in *2016 European Intelligence and Security Informatics Conference*, Aug 2016, pp. 184–187.
[45] R. Kumar, V. V. Phoha, and A. Serwadda, "Continuous authentication of smartphone users by fusing typing, swiping, and phone movement patterns," in *2016 IEEE 8th International Conference on Biometrics Theory, Applications and Systems (BTAS)*, Sep. 2016, pp. 1–8.
[46] Carnegie Mellon University, "Motion Capture Database," http://mocap.cs.cmu.edu/, 2003.
[47] H. C. Volaka, G. Alptekin, O. E. Basar, M. Isbilen, and O. D. Incel, "Towards continuous authentication on mobile phones using deep learning models," *Procedia Computer Science*, vol. 155, pp. 177–184, 2019.
[48] M. Abuhamad, T. Abuhmed, D. Mohaisen, and D. Nyang, "Autosen: Deep-learning-based implicit continuous authentication using smartphone sensors," *IEEE IoT Journal*, vol. 7, no. 6, June 2020.
[49] "Apple introduces iphone xr," https://www.apple.com/newsroom/2018/09/apple-introduces-iphone-xr/, accessed: 2023-11-20.
[50] "Vicon, oxford metrics, oxford, uk - full body modeling with plug-in gait," https://docs.vicon.com/display/Nexus212/Full+body+modeling+with+Plug-in+Gait, accessed: 2023-11-20.
[51] S. Schreven, P. J. Beek, and J. B. Smeets, "Optimising filtering parameters for a 3d motion analysis system," *Journal of Electromyography and Kinesiology*, vol. 25, no. 5, pp. 808–814, 2015.
[52] A. Ferrari, M. G. Benedetti, E. Pavan, C. Frigo, D. Bettinelli, M. Rabuffetti, P. Crenna, and A. Leardini, "Quantitative comparison of five current protocols in gait analysis," *Gait and Posture*, vol. 28, no. 2, 2008.
[53] I. Roupa, M. R. da Silva, F. Marques, S. B. Gonçalves, P. Flores, and M. T. da Silva, "On the modeling of biomechanical systems for human movement analysis: a narrative review," *Archives of Computational Methods in Engineering*, vol. 29, no. 7, pp. 4915–4958, 2022.
[54] A. D. Sylvester, S. G. Lautzenheiser, and P. A. Kramer, "A review of musculoskeletal modelling of human locomotion," *Interface Focus*, vol. 11, no. 5, p. 20200060, 2021.
[55] A. Leardini, Z. Sawacha, G. Paolini, S. Ingrosso, R. Nativo, and M. G. Benedetti, "A new anatomically based protocol for gait analysis in children," *Gait and Posture*, vol. 26, no. 4, pp. 560–571, 2007.
[56] L. Araújo, L. Sucupira, M. Lizarraga, L. Ling, and J. Yabu-uti, "User authentication through typing biometrics features," in *Intl. Conference Biometric Authentication*, vol. 3072, 01 2004, pp. 694–700.
[57] R. Vert, J.-P. Vert, and B. Schölkopf, "Consistency and convergence rates of one-class svms and related algorithms." *Journal of Machine Learning Research*, vol. 7, no. 5, 2006.
[58] L. Breiman, "Random forests," *Machine Learning*, vol. 45, no. 1, pp. 5–32, Oct 2001.
[59] Z. Zhang, "Introduction to machine learning: k-nearest neighbors," *Annals of translational medicine*, vol. 4, no. 11, 2016.
[60] R. Kumar, P. P. Kundu, D. Shukla, and V. V. Phoha, "Continuous user authentication via unlabeled phone movement patterns," in *2017 IEEE International Joint Conference on Biometrics*, 2017, pp. 177–184.
[61] F. Pedregosa, G. Varoquaux, A. Gramfort, V. Michel, B. Thirion, O. Grisel, M. Blondel, P. Prettenhofer, R. Weiss, V. Dubourg, J. Vanderplas, A. Passos, D. Cournapeau, M. Brucher, M. Perrot, and E. Duchesnay, "Scikit-learn: Machine learning in Python," *Journal of Machine Learning Research*, vol. 12, pp. 2825–2830, 2011.
[62] M. Amer, M. Goldstein, and S. Abdennadher, "Enhancing one-class support vector machines for unsupervised anomaly detection," in *Proceedings of the ACM SIGKDD workshop on outlier detection and description*, 2013, pp. 8–15.
[63] F. T. Liu, K. M. Ting, and Z.-H. Zhou, "Isolation forest," in *2008 eighth ieee international conference on data mining*. IEEE, 2008, pp. 413–422.
[64] M. E. Tipping and C. M. Bishop, "Mixtures of Probabilistic Principal Component Analyzers," *Neural Computation*, vol. 11, no. 2, pp. 443–482, 02 1999.

[65] J. Tian, H. Gu, C. Gao, and J. Lian, "Local density one-class support vector machines for anomaly detection," *Nonlinear Dynamics*, vol. 64, pp. 127–130, 2011.

[66] C. Liang, C. Yu, X. Wei, X. Xu, Y. Hu, Y. Wang, and Y. Shi, "Auth+ track: Enabling authentication free interaction on smartphone by continuous user tracking," in *Proceedings of the 2021 CHI Conference on Human Factors in Computing Systems*, 2021, pp. 1–16.

[67] K. Ahuja, S. Mayer, M. Goel, and C. Harrison, "Pose-on-the-go: Approximating user pose with smartphone sensor fusion and inverse kinematics," in *Proceedings of the 2021 CHI Conference on Human Factors in Computing Systems*, 2021, pp. 1–12.

[68] D. Kim, K. Park, and G. Lee, "Oddeyecam: A sensing technique for body-centric peephole interaction using wfov rgb and nfov depth cameras," in *Proceedings of the 33rd Annual ACM Symposium on User Interface Software and Technology*, 2020, pp. 85–97.

[69] D. Tome, T. Alldieck, P. Peluse, G. Pons-Moll, L. Agapito, H. Badino, and F. De la Torre, "Selfpose: 3d egocentric pose estimation from a headset mounted camera," *IEEE Transactions on Pattern Analysis and Machine Intelligence*, vol. 45, no. 6, pp. 6794–6806, 2020.

[70] T. Babic, F. Perteneder, H. Reiterer, and M. Haller, "Simo: Interactions with distant displays by smartphones with simultaneous face and world tracking," in *Extended Abstracts of the 2020 CHI Conference on Human Factors in Computing Systems*, 2020, pp. 1–12.

[71] X. Chen, J. Schwarz, C. Harrison, J. Mankoff, and S. Hudson, "Around-body interaction: sensing & interaction techniques for proprioception-enhanced input with mobile devices," in *Proceedings of the 16th international conference on Human-computer interaction with mobile devices & services*, 2014, pp. 287–290.

[72] K. Ahuja, C. Harrison, M. Goel, and R. Xiao, "Mecap: Whole-body digitization for low-cost vr/ar headsets," in *Proc. of the 32nd Annual ACM Symposium on User Interface Software and Tech.*, 2019.

[73] W. Xu, A. Chatterjee, M. Zollhoefer, H. Rhodin, P. Fua, H.-P. Seidel, and C. Theobalt, "Mo 2 cap 2: Real-time mobile 3d motion capture with a cap-mounted fisheye camera," *IEEE transactions on visualization and computer graphics*, vol. 25, no. 5, pp. 2093–2101, 2019.

[74] V. Mollyn, R. Arakawa, M. Goel, C. Harrison, and K. Ahuja, "Imuposer: Full-body pose estimation using imus in phones, watches, and earbuds," in *Proceedings of the 2023 CHI Conference on Human Factors in Computing Systems*, 2023, pp. 1–12.

[75] S. Mahmud, K. Li, G. Hu, H. Chen, R. Jin, R. Zhang, F. Guimbretière, and C. Zhang, "Posesonic: 3d upper body pose estimation through egocentric acoustic sensing on smartglasses," *Proc. of the ACM on Interactive, Mobile, Wearable and Ubiquitous Tech.*, vol. 7, no. 3, 2023.

[76] H. Lim, Y. Li, M. Dressa, F. Hu, J. H. Kim, R. Zhang, and C. Zhang, "Bodytrak: Inferring full-body poses from body silhouettes using a miniature camera on a wristband," *Proc. of the ACM on Interactive, Mobile, Wearable and Ubiquitous Technologies*, vol. 6, no. 3, 2022.

[77] W. Wei, K. Kurita, J. Kuang, and A. Gao, "Real-time 3d arm motion tracking using the 6-axis imu sensor of a smartwatch," in *2021 IEEE Intl. Conf. on Wearable and Implantable Body Sensor Networks*, 2021.

[78] P. Streli, R. Armani, Y. F. Cheng, and C. Holz, "Hoov: Hand out-of-view tracking for proprioceptive interaction using inertial sensing," in *Proceedings of the 2023 CHI Conference on Human Factors in Computing Systems*, 2023, pp. 1–16.

[79] S. Shen, H. Wang, and R. Roy Choudhury, "I am a smartwatch and i can track my user's arm," in *Proceedings of the 14th annual intl. conference on Mobile systems, applications, and services*, 2016, pp. 85–96.

[80] J. A. B. Madrigal, L. A. C. Rodríguez, E. C. Pérez, P. R. H. Rodríguez, and H. Sossa, "Hip and lower limbs 3d motion tracking using a double-stage data fusion algorithm for imu/marg-based wearables sensors," *Biomedical Signal Processing and Control*, vol. 86, p. 104938, 2023.

Kiran S. Balagani is currently an Associate Professor of Computer Science at New York Institute of Technology. His research interests are in anomaly detection, behavioral biometrics, and privacy-preserving biometrics. His research has been sponsored by the National Science Foundation and DARPA. He received the Ph.D. degree from Louisiana Tech University, USA.

Nicholas Cariello is currently a Ph.D. Candidate in Computer Science at the New York Institute of Technology. His research interests include behavioral biometrics, machine learning, deep learning, artificial intelligence, and privacy-preserving biometrics. He expresses gratitude to his employer, IBM for their support o f his doctoral research. He received his B.S. and M.S. degree in Computer Science from New York Institute of Technology, USA.

Rob Eslinger graduated from Holy Cross College in Worcester, MA with a double bachelor degree in Mathematics and Physics. He received his Master's in Cybersecurity from NYIT in 2021. He is interested in cybersecurity, cryptography and information science.

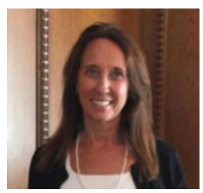

Rosemary Gallagher is an associate professor at NYIT's Doctor of Physical Therapy Program. Gallagher graduated from Colorado State University in 1983 with a B.S. in Physical Education and has earned a B.S. in Physical Therapy in 1989 and a Clinical Doctorate in Physical Therapy in 2008 from Stony Brook University. She holds a Ph.D. from Rutgers University. She has over 30 years of clinical experience with a variety of patient populations including geriatric, neurologic, and orthopedic patients.

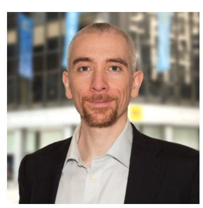

Paolo Gasti is an Associate Professor of Computer Science at NYIT. His work focuses on behavioral biometrics, privacy-preserving biometric authentication, secure multi-party protocols, and network security. His research has been sponsored by the National Science Foundation and the DARPA. He received his B.S., M.S., and Ph.D. degrees from University of Genoa, Italy. Before joining NYIT, he worked as a research scholar at University of California, Irvine.

Isaac Kurtzer is currently an Assistant Professor in the Biomedical Science Department of New York Institute of Technology – College of Osteopathic Medicine. He received his PhD in Neuroscience from Brandeis University (Waltham, MA) and completed a post-doctoral fellowship at Queen's University (Kingston, ON). His research on sensori-motor control has addressed motor learning, stretch reflexes, motor cortical processing, and rapid decision-making. He also teaches human neuroanatomy and biostatistics to the university's medical students.

APPENDIX

TABLE VII
MUTUAL INFORMATION (MI) OF TOP CUMULATIVE FEATURES FOR SITTING

Rank	Feature	MI	Rank	Feature	MI	Rank	Feature	MI
1	Left Ankle -Theta Angle	3.2775	32	Lower Spine -Phi Angle	1.9806	63	Velocity of Swipe	0.3301
2	Right Ankle -Theta Angle	3.2384	33	Right Elbow -Phi Angle	1.9781	64	Gyro x Mean	0.3152
3	Left Knee -Phi Angle	3.2149	34	Neck -Phi Angle	1.9388	65	Gyro y Min	0.3134
4	Right Knee -Phi Angle	3.1557	35	Left Wrist -Phi Angle	1.9350	66	Gyro x Energy	0.3012
5	Left Ankle -Phi Angle	3.0773	36	Left Wrist -Theta Angle	1.8514	67	Gyro x Max	0.2751
6	Right Ankle -Phi Angle	3.0610	37	Right Shoulder -Phi Angle	1.8216	68	Gyro y SD	0.2594
7	Right Hip(leg) -Theta Angle	3.0497	38	Head Phone distance	1.8125	69	Gyro x Min	0.2534
8	Left Hip(leg) -Theta Angle	3.0220	39	Neck -Theta Angle	1.8004	70	Accel x SD	0.2492
9	Left Knee -Theta Angle	3.0191	40	Clavicle to Phone distance	1.7912	71	Accel y SD	0.2426
10	Right Knee -Theta Angle	2.9635	41	Sternum to Phone distance	1.7898	72	Gyro x SD	0.2343
11	Left Hip(leg) -Phi Angle	2.9414	42	Right Wrist -Phi Angle	1.7771	73	Accel y Entropy	0.2203
12	Right Hip(leg) -Phi Angle	2.9384	43	Right Shoulder to Phone distance	1.7405	74	Accel x Entropy	0.2154
13	Left Hip to Left Elbow distance	2.7290	44	Right Shoulder -Theta Angle	1.6635	75	Accel z Entropy	0.2134
14	Right Hip to Left Elbow distance	2.7215	45	Right Elbow -Theta Angle	1.6492	76	Accel z SD	0.1950
15	Clavicle to Left Elbow distance	2.7106	46	Head to Phone -Theta Angle	1.6349	77	Time Duration of Swipe	0.1949
16	Sternum to Left Elbow distance	2.6311	47	Right Wrist -Theta Angle	1.3753	78	Gyro z Energy	0.1818
17	Upper Spine -Phi Angle	2.5278	48	Accel y Mean	0.8877	79	Gyro z SD	0.1781
18	Lower Spine -Theta angle	2.4447	49	Accel y Max	0.7899	80	Gyro x Entropy	0.1728
19	Left Hip to Right Elbow distance	2.4242	50	Accel y Min	0.7757	81	Gyro z Mean	0.1709
20	Right Hip to Right Elbow distance	2.3134	51	Accel z Mean	0.6930	82	Gyro y Entropy	0.1706
21	Left Shoulder -Phi Angle	2.2827	52	Accel y Energy	0.6382	83	Gyro z Entropy	0.1682
22	Left Elbow -Phi Angle	2.2788	53	Accel z Max	0.5855	84	Gyro z Max	0.1628
23	Clavicle to Right Elbow distance	2.2524	54	Accel x Mean	0.5591	85	Angular Sum of Swipe	0.1596
24	Left Shoulder -Theta Angle	2.2143	55	Accel x Max	0.5572	86	Gyro z Min	0.1595
25	Upper Spine -Theta Angle	2.2006	56	Accel z Min	0.5494	87	Accel y Kurtosis	0.0404
26	Left Hip to Phone distance	2.1602	57	Accel x Energy	0.4587	88	Gyro x Kurtosis	0.0339
27	Left Elbow -Theta Angle	2.0937	58	Accel x Min	0.4585	89	Accel x Kurtosis	0.0325
28	Left Shoulder to Phone distance	2.0775	59	Accel z Energy	0.4208	90	Accel z Kurtosis	0.0279
29	Right Hip to Phone distance	2.0665	60	Gyro y Mean	0.3814	91	Gyro y Kurtosis	0.0278
30	Sternum to Right Elbow distance	2.0406	61	Gyro y Energy	0.3791	92	Length of Swipe	0.0217
31	Head to Phone -Phi Angle	2.0311	62	Gyro y Max	0.3399	93	Gyro z Kurtosis	0.0159

TABLE VIII
MUTUAL INFORMATION (MI) OF TOP CUMULATIVE FEATURES FOR WALKING

Rank	Feature	MI	Rank	Feature	MI	Rank	Feature	MI
1	Clavicle to Left Elbow distance	2.1658	32	Left Shoulder -Phi Angle	1.2838	63	Accel y Entropy	0.1962
2	Clavicle to Right Elbow distance	2.1585	33	Right Shoulder -Phi Angle	1.2577	64	Gyro y Min	0.1916
3	Sternum to Left Elbow distance	1.9829	34	Head to Phone -Phi Angle	1.2562	65	Accel x Entropy	0.1899
4	Right Hip to Left Elbow distance	1.8950	35	Neck -Phi Angle	1.1762	66	Time Duration of Swipe	0.1856
5	Sternum to Right Elbow distance	1.8790	36	Right Hip(leg) -Theta Angle	1.0918	67	Gyro y Mean	0.1855
6	Left Hip to Right Elbow distance	1.7596	37	Left Hip(leg) -Theta Angle	1.0595	68	Gyro x Energy	0.1833
7	Left Hip to Left Elbow distance	1.7564	38	Right Knee -Theta Angle	0.8329	69	Gyro x Entropy	0.1777
8	Right Hip to Right Elbow distance	1.7121	39	Lower Spine -Theta angle	0.8109	70	Gyro y Max	0.1754
9	Left Shoulder to Phone distance	1.6542	40	Left Knee -Theta Angle	0.7973	71	Gyro y Entropy	0.1732
10	Left Ankle -Theta Angle	1.6438	41	Lower Spine -Phi Angle	0.7797	72	Accel x Energy	0.1671
11	Right Elbow -Theta Angle	1.6387	42	Left Hip(leg) -Phi Angle	0.6494	73	Gyro x SD	0.1651
12	Left Wrist -Theta Angle	1.6269	43	Left Ankle -Phi Angle	0.6363	74	Gyro z Entropy	0.1644
13	Left Elbow -Phi Angle	1.6247	44	Right Hip(leg) -Phi Angle	0.6111	75	Gyro x Mean	0.1635
14	Right Ankle -Theta Angle	1.6141	45	Right Ankle -Phi Angle	0.5120	76	Gyro x Max	0.1557
15	Left Elbow -Theta Angle	1.5946	46	Accel y Mean	0.4498	77	Accel z SD	0.1511
16	Left Hip to Phone distance	1.5642	47	Accel y Min	0.3847	78	Angular Sum of Swipe	0.1418
17	Neck -Theta Angle	1.5407	48	Accel y Max	0.3469	79	Gyro x Min	0.1371
18	Right Hip to Phone distance	1.5371	49	Left Knee -Phi Angle	0.3365	80	Gyro z SD	0.1337
19	Right Wrist -Phi Angle	1.5003	50	Right Knee -Phi Angle	0.3337	81	Accel y SD	0.1267
20	Left Wrist -Phi Angle	1.4892	51	Velocity of Swipe	0.3030	82	Accel x SD	0.1129
21	Left Shoulder -Theta Angle	1.4824	52	Accel y Energy	0.2779	83	Gyro z Energy	0.1066
22	Right Elbow -Phi Angle	1.4669	53	Accel z Mean	0.2612	84	Gyro z Max	0.0990
23	Head Phone distance	1.4652	54	Accel z Max	0.2435	85	Gyro z Mean	0.0850
24	Upper Spine -Theta Angle	1.4554	55	Accel x Mean	0.2356	86	Gyro z Min	0.0842
25	Head to Phone -Theta Angle	1.4319	56	Accel z Min	0.2340	87	Gyro x Kurtosis	0.0396
26	Right Shoulder -Theta Angle	1.4254	57	Gyro y Energy	0.2261	88	Accel x Kurtosis	0.0387
27	Sternum to Phone distance	1.4235	58	Accel x Max	0.2129	89	Gyro y Kurtosis	0.0362
28	Clavicle to Phone distance	1.4179	59	Accel x Min	0.2060	90	Accel z Kurtosis	0.0342
29	Right Shoulder to Phone distance	1.3992	60	Accel z Entropy	0.2039	91	Accel y Kurtosis	0.0281
30	Right Wrist -Theta Angle	1.3601	61	Accel z Energy	0.2006	92	Length of Swipe	0.0176
31	Upper Spine -Phi Angle	1.3335	62	Gyro y SD	0.1996	93	Gyro z Kurtosis	0.0123

TABLE IX
EERS FOR BASELINE DATA AND MOTION CAPTURE DATA FOR EACH REGION, SPLIT BY BODY MOTION TYPE FOR EACH CLASSIFIERS.

Method	**Posture**	**Feature Set**	**Window Length in Seconds**								
			1	**2**	**3**	**5**	**10**	**15**	**20**	**30**	**60**
SM	Walk	Baseline Only	0.396	0.327	0.290	0.239	0.186	0.165	0.148	0.139	0.105
		Upper Region Only	0.246	0.171	0.152	0.131	0.114	0.108	0.098	0.098	0.085
		Center Region Only	0.201	0.104	0.086	0.061	0.049	0.039	0.035	0.034	0.025
		Lower Region Only	0.272	0.191	0.168	0.140	0.119	0.109	0.103	0.090	0.083
	Sit	Baseline Only	0.337	0.269	0.239	0.207	0.164	0.150	0.140	0.123	0.115
		Upper Region Only	0.216	0.155	0.143	0.124	0.105	0.101	0.101	0.093	0.091
		Center Region Only	0.210	0.142	0.129	0.106	0.086	0.082	0.082	0.079	0.079
		Lower Region Only	0.226	0.174	0.165	0.146	0.133	0.130	0.130	0.128	0.126
OSVM	Walk	Baseline Only	0.422	0.378	0.338	0.297	0.258	0.240	0.228	0.236	0.232
		Upper Region Only	0.246	0.242	0.227	0.211	0.252	0.229	0.215	0.209	0.186
		Center Region Only	0.140	0.137	0.195	0.175	0.168	0.150	0.139	0.131	0.135
		Lower Region Only	0.266	0.246	0.233	0.250	0.222	0.206	0.179	0.180	0.171
	Sit	Baseline Only	0.323	0.296	0.272	0.254	0.218	0.210	0.202	0.226	0.209
		Upper Region Only	0.233	0.228	0.222	0.220	0.207	0.201	0.223	0.217	0.201
		Center Region Only	0.207	0.235	0.211	0.209	0.205	0.217	0.224	0.222	0.230
		Lower Region Only	0.207	0.203	0.200	0.195	0.200	0.200	0.197	0.207	0.191
RF	Walk	Baseline Only	0.237	0.219	0.207	0.197	0.181	0.173	0.167	0.165	0.161
		Upper Region Only	0.133	0.134	0.131	0.134	0.130	0.142	0.146	0.146	0.172
		Center Region Only	0.085	0.082	0.081	0.083	0.095	0.097	0.098	0.110	0.125
		Lower Region Only	0.168	0.172	0.168	0.162	0.162	0.160	0.164	0.161	0.180
	Sit	Baseline Only	0.197	0.182	0.172	0.163	0.156	0.147	0.144	0.136	0.140
		Upper Region Only	0.117	0.125	0.131	0.127	0.136	0.129	0.133	0.130	0.143
		Center Region Only	0.093	0.080	0.112	0.100	0.114	0.114	0.122	0.132	0.119
		Lower Region Only	0.159	0.147	0.146	0.164	0.163	0.162	0.161	0.169	0.178
KNN	Walk	Baseline Only	0.430	0.425	0.417	0.405	0.388	0.384	0.380	0.371	0.358
		Upper Region Only	0.203	0.214	0.217	0.226	0.217	0.232	0.247	0.241	0.221
		Center Region Only	0.155	0.162	0.168	0.162	0.155	0.147	0.159	0.175	0.181
		Lower Region Only	0.198	0.209	0.207	0.202	0.196	0.192	0.206	0.201	0.204
	Sit	Baseline Only	0.421	0.414	0.415	0.412	0.401	0.384	0.356	0.361	0.326
		Upper Region Only	0.234	0.233	0.240	0.247	0.248	0.244	0.248	0.249	0.251
		Center Region Only	0.198	0.199	0.212	0.215	0.229	0.229	0.229	0.232	0.255
		Lower Region Only	0.240	0.236	0.229	0.225	0.221	0.215	0.210	0.209	0.206

This section presents updated authentication results, based on the use of a different type of content-aware alignment algorithm between the phone's motion sensor data and the motion capture system. Specifically, we used the motion-capture sensors placed on the smartphone to align the phone's motion sensor data with the motion capture data. This improved alignment reduces inaccuracies in the feature extraction process. By addressing this misalignment, the phone and body movement data are now better synchronized, resulting in more accurate features, which in turn led to reduced EERs across different classifiers and body-motion types.

Table IX present the Equal Error Rates (EERs) for baseline data, which includes smartphone swipe and phone-movement data, and compares it with motion capture data for each body region (upper, center, lower) during different activities (sitting or walking) across varying classifiers and time windows (1-60 seconds). Table X presents the decrease in Equal Error Rates (EERs) when comparing the baseline features (e.g., smartphone swipe and phone-movement data) to the feature-level fusion of baseline features with posture and body movement features. This comparison is performed using different classifiers.

While these changes improve overall accuracies the main conclusions of the paper remain unchanged, i.e., posture and body movement features can reduce error rates and authentication latencies to as low as 1-5 seconds. The improvements seen in Table IX, X confirm and strengthen the original conclusions by showing even lower error rates as a result of more accurate alignment.

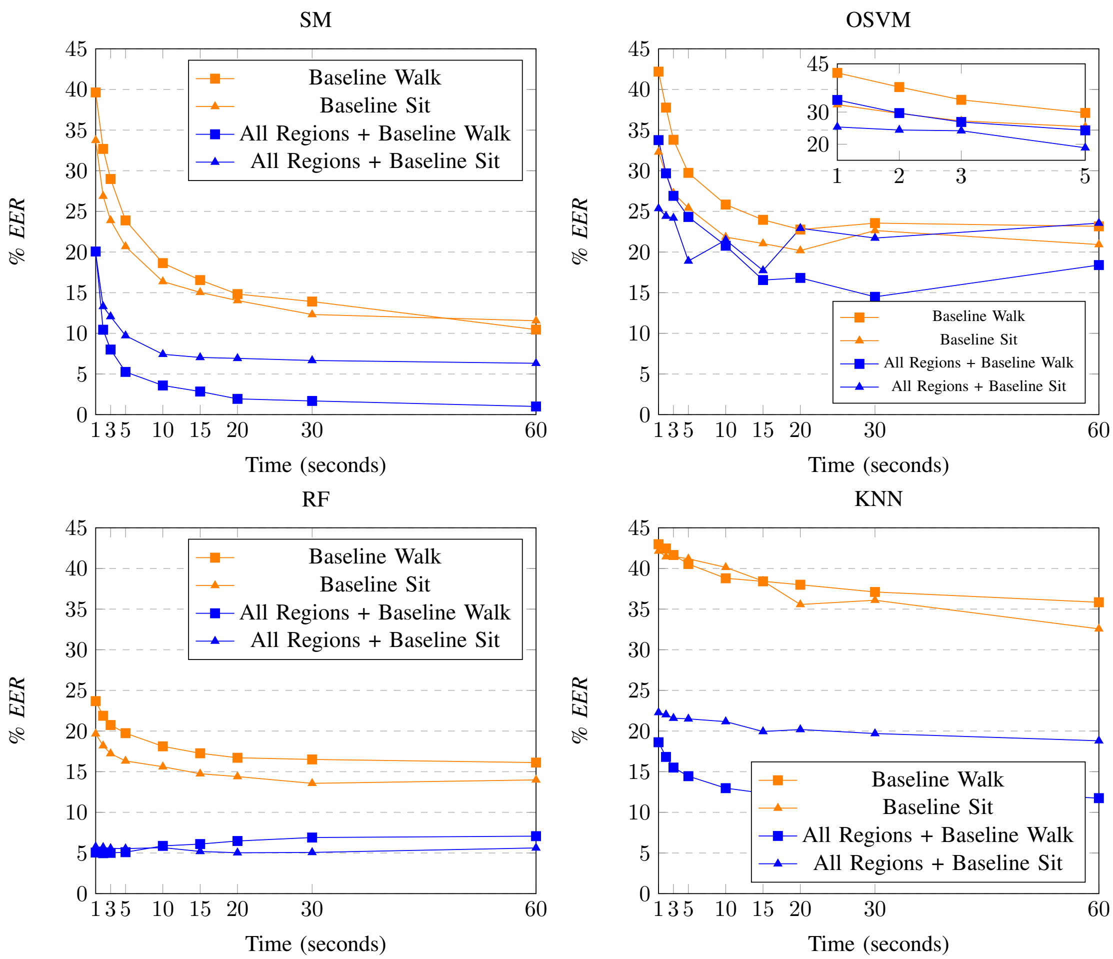

Fig. 6. EERs of baseline features vs. feature-level fusion of posture and body movement features from all regions in sit and walk conditions for each verifier.

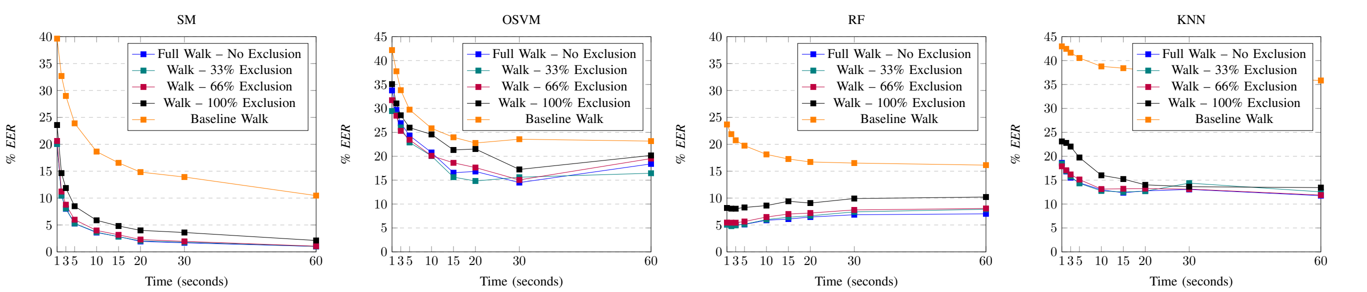

Fig. 7. Feature-level fusion results with each classifier for 33%-, 66%-, and 100%-exclusion features sets (Table VI) as compared to no exclusion, and the baseline for walking posture.

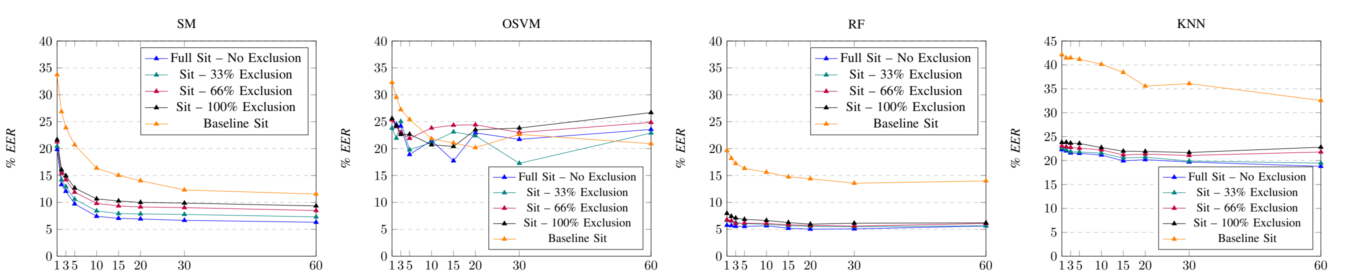

Fig. 8. Feature-level fusion results with each verifier for 33%-, 66%-, and 100%-exclusion features sets (Table VI) as compared to no exclusion, and the baseline for sitting posture.

TABLE X
DECREASE IN EERS BETWEEN BASELINE FEATURES AND FEATURE-LEVEL FUSION OF BASELINE WITH POSTURE AND BODY MOVEMENT FEATURES USING VARYING CLASSIFIERS. POSITIVE NUMBERS INDICATE A DECREMENT OF EER COMPARED TO THE BASELINE.

Method	Posture	Feature-level Fusion	Window Length in Seconds								
			1	2	3	5	10	15	20	30	60
SM	Walk	Upper Region + Baseline	0.117	0.133	0.130	0.118	0.099	0.096	0.084	0.086	0.068
		Center Region + Baseline	0.174	0.197	0.187	0.167	0.136	0.128	0.117	0.112	0.090
		Lower Region + Baseline	0.110	0.131	0.126	0.116	0.104	0.096	0.093	0.094	0.079
		All Regions + Baseline	0.196	0.222	0.210	0.186	0.150	0.137	0.129	0.122	0.095
	Sit	Upper Region + Baseline	0.110	0.106	0.097	0.090	0.072	0.069	0.065	0.049	0.057
		Center Region + Baseline	0.123	0.120	0.107	0.099	0.082	0.076	0.072	0.058	0.057
		Lower Region + Baseline	0.115	0.100	0.082	0.070	0.047	0.038	0.031	0.018	0.014
		All Regions + Baseline	0.139	0.136	0.118	0.110	0.089	0.080	0.071	0.057	0.052
OSVM	Walk	Upper Region + Baseline	0.056	0.051	0.035	0.019	0.021	0.017	0.026	0.034	0.024
		Center Region + Baseline	0.119	0.115	0.116	0.088	0.086	0.078	0.078	0.098	0.076
		Lower Region + Baseline	0.021	0.028	0.034	0.030	0.042	0.039	0.052	0.082	0.044
		All Regions + Baseline	0.084	0.081	0.069	0.054	0.051	0.074	0.059	0.091	0.048
	Sit	Upper Region + Baseline	0.038	0.042	0.028	0.023	0.016	0.015	0.016	-0.008	-0.009
		Center Region + Baseline	0.064	0.053	0.050	0.033	0.017	0.029	0.029	-0.007	-0.034
		Lower Region + Baseline	0.077	0.064	0.053	0.044	0.026	0.016	0.020	0.010	-0.009
		All Regions + Baseline	0.069	0.051	0.031	0.065	0.004	0.033	-0.027	0.009	-0.026
RF	Walk	Upper Region + Baseline	0.115	0.104	0.094	0.085	0.076	0.066	0.060	0.053	0.051
		Center Region + Baseline	0.161	0.150	0.137	0.123	0.098	0.084	0.077	0.066	0.059
		Lower Region + Baseline	0.102	0.092	0.086	0.083	0.072	0.055	0.051	0.046	0.044
		All Regions + Baseline	0.186	0.169	0.157	0.146	0.122	0.112	0.102	0.096	0.091
	Sit	Upper Region + Baseline	0.096	0.080	0.072	0.062	0.055	0.042	0.045	0.041	0.039
		Center Region + Baseline	0.135	0.117	0.107	0.093	0.083	0.076	0.073	0.062	0.060
		Lower Region + Baseline	0.076	0.069	0.068	0.066	0.063	0.063	0.054	0.046	0.048
		All Regions + Baseline	0.139	0.125	0.117	0.108	0.100	0.096	0.094	0.085	0.084
KNN	Walk	Upper Region + Baseline	0.182	0.172	0.161	0.164	0.167	0.180	0.176	0.185	0.179
		Center Region + Baseline	0.240	0.219	0.212	0.213	0.231	0.250	0.256	0.259	0.245
		Lower Region + Baseline	0.188	0.189	0.188	0.192	0.204	0.215	0.206	0.216	0.201
		All Regions + Baseline	0.244	0.256	0.261	0.261	0.258	0.261	0.252	0.241	0.241
	Sit	Upper Region + Baseline	0.188	0.179	0.177	0.179	0.178	0.163	0.140	0.136	0.090
		Center Region + Baseline	0.215	0.202	0.195	0.190	0.185	0.166	0.138	0.130	0.085
		Lower Region + Baseline	0.208	0.208	0.212	0.214	0.204	0.198	0.174	0.177	0.137
		All Regions + Baseline	0.199	0.194	0.199	0.197	0.190	0.185	0.154	0.164	0.138